

LONG TERM EVOLUTION OF MAGNETIC TURBULENCE IN RELATIVISTIC COLLISIONLESS SHOCKS: ELECTRON-POSITRON PLASMAS

PHILIP CHANG^{1,2,3}, ANATOLY SPITKOVSKY⁴, AND JONATHAN ARONS^{1,2,5,6}

Draft version September 3, 2021

ABSTRACT

We study the long term evolution of magnetic fields generated by a collisionless relativistic e^+e^- shock which is initially unmagnetized. Our 2D particle-in-cell numerical simulations show that downstream of such a Weibel-mediated shock, particle distributions are close to isotropic, relativistic Maxwellians, and the magnetic turbulence is highly intermittent spatially. The non-propagating magnetic fields in the turbulence form relatively isolated regions with transverse dimension $\sim 10 - 20$ skin depths. These structures decay in amplitude, with little sign of downstream merging. The fields start with magnetic energy density $\sim (0.1 - 0.2)$ of the upstream kinetic energy within the shock transition, but rapid downstream decay drives the fields to much smaller values, below 10^{-3} of equipartition after $\sim 10^3$ skin depths.

In an attempt to construct a theory that follows field decay to these smaller values, we explore the hypothesis that the observed damping is a variant of Landau damping in an unmagnetized plasma. The model is based on the small value of the downstream magnetic energy density, which suggests that particle orbits are only weakly perturbed from straight line motion, if the turbulence is homogeneous. Using linear kinetic theory applied to electromagnetic fields in an isotropic, relativistic Maxwellian plasma, we find a simple analytic form for the damping rates, γ_k , in two and three dimensions for small amplitude, subluminal electromagnetic fields. We find that magnetic energy does damp due to phase mixing of current carrying particles as $(\omega_p t)^{-q}$ with $q \sim 1$. This overall decay compares well to that found in simulations, since it depends primarily on the longest wavelength modes, $kc/\omega_p \ll 1$. However, the theory predicts overly rapid damping of short wavelength modes. We speculate that magnetic trapping of a substantial fraction of the particles within the highly spatially intermittent downstream magnetic structures may be the origin of this discrepancy. In addition, trapping may form the basis for MHD-like behavior, permitting a small fraction of the initial magnetic energy to persist for times much greater than have been followed in the simulations.

We briefly speculate on other physical processes, which depend on the presence of suprathermal particles, that may cause the generation of longer wavelength magnetic fields that create a magnetized plasma ($kr_{Larmor} \ll 1$), in which the damping is not as fast. However, absent such additional physical processes, we conclude that initially unmagnetized relativistic shocks in electron-positron plasmas are unable to form persistent downstream magnetic fields. These results put interesting constraints on synchrotron models for the prompt and afterglow emission from GRBs. We also comment on the relevance of these results for relativistic shocks in electron-ion plasmas.

Subject headings: shock waves – turbulence – gamma ray: bursts – plasmas

1. INTRODUCTION

The prompt emission and afterglows of gamma-ray bursts (GRBs) may be manifestations of ultrarelativistic shock waves, propagating in media where the large scale upstream magnetization is too weak to affect the shock structure, and too weak, if simply compressed by the shock, to provide the magnetization inferred from synchrotron models of the burst emission (see Piran 2005ab and references therein). The weakly magnetized outflows in the rotational equators of rotation powered pulsars (Coroniti 1990) may also be sites of essentially unmagne-

tized shock waves terminating the relativistic winds in a region which occupies a finite latitude band with respect to the rotational equator of the underlying neutron star. Yet the radiation from these systems has been modeled as being due to synchrotron radiation, which requires the presence of a magnetic field strong enough to deflect particles through a substantial fraction of their Larmor orbits. At the very least, this requires magnetic structures with amplitude, δB , whose characteristic dimensions, R_B , are comparable to or larger than $mc^2/e\delta B$, for all particle energies inferred to contribute to the observed radiation.

Unmagnetized anisotropic plasmas spontaneously generate small-scale magnetic fields via the Weibel instability (Weibel 1959). Shocks have strong plasma anisotropy in the transition layer separating the upstream and downstream media, as well as in the foreshock where downstream particles escape into the upstream, which provides the free energy for generating magnetic fields with spatial scales on the order of the plasma skin depth, c/ω_p , where ω_p is the plasma frequency. Medvedev

¹ Department of Astronomy, Campbell Hall, University of California, Berkeley, CA 94720; pchang@astro.berkeley.edu, arons@astro.berkeley.edu

² Theoretical Astrophysics Center

³ Miller Institute for Basic Research

⁴ Department of Astrophysical Sciences, Peyton Hall, Princeton University, Princeton, NJ: anatoly@astro.princeton.edu

⁵ Department of Physics, LeConte Hall, University of California, Berkeley, CA 94720

⁶ Kavli Institute for Particle Astrophysics and Cosmology, Stanford University

and Loeb (1999) and Gruzinov and Waxman (1999) argued that the relativistic form of this instability (Yoon & Davidson 1987) could macroscopically magnetize the downstream plasma where the GRB radiation arises (Larmor radii small compared to flow scale). Through numerical and analytic studies, they and various authors (Silva *et al.* 2003, Medvedev *et al.* 2005) have argued that the instability forms filaments of electric current and B field. These filaments merge and cause magnetic energy to cascade from the initial microscopic scale $\sim c/\omega_p$ to larger scales. Thus, the filamented plasma becomes magnetized with a B field hypothesized to survive throughout a large fraction of the shocked medium.

Such inverse cascades have been observed in 2D and 3D particle-in-cell simulations in the *foreshock* region, the part of the shock structure where the upstream and downstream media interpenetrate and the stream filamentation modes grow from noise with most incoming particles still undeflected from the upstream flow. Simulations show that current filaments merge and grow in amplitude until they reach the magnetic trapping limit, where the filament currents and their magnetic fields become comparable to the Alfvén limit (Davidson *et al.* 1972; Kato 2005; also see Milosavljevic, Nakar, & Spitkovsky 2006; Milosavljevic & Nakar 2006a). At that point the particles' orbits on the filament boundaries become chaotic, the filaments disorganize, and scattering from the disorganized magnetic fluctuations halts the streaming of the bulk of the plasma, isotropizing and thermalizing the flow, all within a layer tens to hundreds of skin depths thick (Spitkovsky 2005), in accord with Kato (2005)'s model for shock formation. The magnetic energy is as high as 10-20% of the bulk plasma flow energy *within this scattering layer*, where the density jump between upstream and downstream occurs.

These initially small-scale B-fields must survive for tens of thousands to millions of inverse plasma periods to serve as the source of the magnetization invoked in synchrotron models of GRB emission (Gruzinov & Waxman 1999; Piran 2005ab; Katz, Keshet, & Waxman 2007). Long-lived fields are also required in Diffusive Fermi Acceleration (DFA) models used to explain the appearance of the nonthermal particle spectra observed through their synchrotron and inverse Compton emission in GRBs, and in pulsar wind nebulae (PWNe) and other sites of nonthermal photon emission in relativistic flows. However, present simulations (Kazimura *et al.* 1998; Silva *et al.* 2003; Frederiksen *et al.* 2004; Hededal *et al.* 2005; Nishikawa *et al.* 2003, 2005) have not followed the flow through the shock transition layer into the downstream region because they employ periodic boundary conditions, are too small, or both. The question of the structure and long-term survival of the B-fields has remained open (see for instance, Gruzinov & Waxman 1999; Gruzinov 2001ab; Medvedev *et al.* 2005).

In this paper, we show via linear theory that the phase mixing between individual particles and organized macroscopic currents implies rapid decay of the magnetic energy in the downstream medium. We begin by briefly describing the essential features of the plasma produced by the shock via numerical simulations in §2. These simulations show the downstream magnetic structures are non-propagating in the frame of the downstream medium, and are intermittent spatially, organized

into clumps and filaments of magnetic field with typical diameter $\sim 10 - 20$ skin depths, immersed into a highly isotropic plasma. In this downstream isotropic Maxwellian particle distribution, we calculate the damping rates from Vlasov linear response theory, assuming the particles are unmagnetized (Larmor radii \gg magnetic clump diameter), recovering a result due to Mikhailovskii (1979) in §3 and Appendix A. Taking snapshots from the simulations as initial conditions, we calculate the decay of the magnetic field as a function of time and position, and compare these theoretical calculations with simulations. We find that the theory does reasonably well in estimating the decay rate of the total magnetic energy as t^{-q} with $q \sim 1$. However, it overestimates the damping rate of shorter wavelength modes. We speculate in §4 that this discrepancy may result from the magnetic trapping of a large fraction of the particles, which suppresses the disorganizing effect of phase mixing on the currents. We also discuss the effects of an inverse cascade on the persistence of magnetic fields, though we find little evidence for its relevance from numerical simulations. We summarize our results and draw some implications for Fermi acceleration and for the magnetization required for synchrotron emission in models of GRBs and other systems in §5.

2. SIMULATION RESULTS

Spitkovsky (2005) and Spitkovsky and Arons (in prep) describe a series of 2D and 3D simulations of relativistic shock waves in e^+e^- plasmas, for varying values of the upstream magnetic field B_1 , including $B_1 = 0$. These are Particle-in-Cell (PIC) simulations (Birdsall and Langdon 1991), using the code *TRISTAN-MP*, developed by one of us (AS). It is a heavily modified descendant of the publicly available code *TRISTAN* (Buneman 1993). We simulate shocks by injecting cold relativistic plasma particles at one end of a large domain and allowing the particles to reflect off a fixed conducting wall at the other end of the box. In this paper, we present 2D calculations utilizing boxes as large as $50,000 \times 2048$ cells with up to 1.35×10^{10} particles which allows us to fully resolve shock formation. Although we track all three velocity and field components, due to the two-dimensional symmetry only particle velocities in the plane of the simulation are non-zero for initially cold flow, and only the out-of-plane component of the magnetic field is excited by in-plane currents. In-plane electrostatic fields are also included.

The interaction of the reflected pair plasma with the incoming stream forms a shock, which propagates toward the plasma injection surface. In the simulations, one plasma skin depth spans 10 cells based on the upstream parameters, i.e., $\lambda_{s1} = c/\omega_{p1} = \sqrt{m_{\pm}c^2\gamma_1/4\pi e^2n_1}$, where n_1 is the upstream total density of electrons and positrons (as measured in the frame of the simulation), ω_{p1} is the upstream plasma frequency, and $\gamma_1 m_{\pm}c^2$ is the upstream flow energy/particle. The time step is $\Delta t = 1/20\omega_{p1}$. In the upstream skin depth units, the largest boxes are then $5000 \times 205 c/\omega_{p1}$. The longest simulation was evolved for $5300\omega_{p1}^{-1}$. We have checked, by using boxes of increasing transverse dimension, that the periodic boundary conditions used on the transverse coordinate do not affect the scale of the magnetic structures formed. In the results exhibited below, we use 64

particles per cell (32 per species) in order to suppress particle noise, which enables us to follow the dynamics of small amplitude fields. We have performed convergence studies, varying the number N of particles per cell from 4 to 64, confirming that the noise level decreases as $1/\sqrt{N}$, while the gross qualities of the shock structure remain the same. Figure 1 shows the snapshots of density and magnetic energy from a typical 2D simulation.⁷ Coordinates are in units of the upstream skin depth, c/ω_{p1} . In the simulation shown, the upstream flow moves to the left with $\gamma_1 = 15$.

Our simulations are large enough to permit the complete development of the shock and show the main features of contemporary collisionless shock simulations even in reduced dimensionality. For instance, we see the factor of ≈ 3.13 increase in density between the upstream and the downstream (Fig. 1c), which is the expected compression factor for this 2D plasma when the plasma properties are measured in the rest frame of the downstream plasma (Gallant *et al.* 1992; Spitkovsky and Arons, in prep). Current filaments (geometrically, these are out-of-plane sheets) show up as the enhancement in plasma density and magnetic energy density in the fore-shock (Fig. 1ab). The scale of the filaments grows towards the shock through merging. The shock is located where the density filaments completely merge and are replaced by a quasi-homogeneous medium. The subject of the saturation of the Weibel instability will be explored in greater detail by Spitkovsky and Arons (in prep).

At the shock transition layer, the filaments disorganize and become clumps of magnetic energy (in 2D the only appreciable magnetic component is the out of plane B_z). Note that these magnetic clumps lose intensity the further downstream they are from the shock (Figure 1b). The magnetic energy peaks before the density completes its rise (as we see in comparing c and d in Fig. 1), i.e., the instability saturates at the Alfvén critical current before the shock fully develops. We also note that the particle distribution function changes from an anisotropic free-streaming population to an isotropic (in the downstream rest frame) thermal population. In the downstream medium, we find that the difference between the perpendicular and parallel momentum is extremely small, $< 1\%$.

As Figures 1 b and d suggest, even though locally in the shock magnetic energy can reach close to equipartition ($\epsilon_B \approx 15\%$ when averaged over the transverse dimension), the magnetic fields decay in the downstream region of the shock. To study this in further detail, we present several cross sections of the plasma at times separated by $450 \omega_{p1}^{-1}$ in Figure 2. Since our simulation is performed in the downstream frame (frame of the reflecting wall), we see the shock propagate through the box at $\approx 0.5c$ (value appropriate for 2D relativistic gas).

Downstream from the shock, the magnetic clumps weaken as a function of time and appear to be non-propagating. In Figure 2, we see this in panels a-d and in the black through blue curves in panel e, which show magnetic energy averaged over the transverse dimension

of the simulation at times from panels a-d. Although the separation between prominent clumps that have larger field strength seems to increase with time, this is due to the faster disappearance of small-scale clumps, presumably due to decay, while the location or size of strong clumps does not significantly evolve. There is little evidence for clump merging far from the shock. In Figure 2 we also plot a vertical line showing the location where we will decompose the magnetic fields into Fourier modes later in §3, in order to study the comparison of the theory of B-field decay with the numerical experiments.

Finally, we mention that 3D shock simulations also show similar behavior (including the lack of substantial downstream merging of magnetic structures) for the shorter times that can be followed with present 3D simulations. Topologically, the magnetic clumps in 2D become large looping structures in 3D. If our 2D plane is thought of as a slice through a 3D simulation, the 3D loops connect field emerging from one clump and returning to another. The orientation of 3D loops would be mostly perpendicular to the original direction of the flow. The particle distribution function is also an isotropic, relativistic Maxwellian in the downstream region.

3. DOWNSTREAM EVOLUTION OF MAGNETIC TURBULENCE

The simulations summarized in §2 suggest that magnetic turbulence decays in the isotropic post-shock plasma. We now attempt to understand this theoretically with the goal of finding a model that allows extrapolation of the magnetic evolution beyond the length of time that can be studied in direct shock simulations. The simulations show that the downstream plasma is isotropic and the downstream particle distribution function is well described by a relativistic Maxwellian. For the purposes of this section, we *assume* the downstream field amplitudes are so small that magnetic trapping is unimportant for almost all particles; therefore, their orbits are almost straight lines. We will revisit this assumption in §4.

We begin by deriving the linear plasma response for electromagnetic fluctuations in an isotropic relativistic plasma with small field fluctuations (Mikhailovskii 1979). The Vlasov equation for each species is

$$\frac{\partial f_s}{\partial t} + \mathbf{v} \cdot \nabla f_s + \frac{q_s}{m_e} \left(\mathbf{E} + \frac{\mathbf{v}}{c} \times \mathbf{B} \right) \cdot \nabla_p f_s = 0. \quad (1)$$

Here, s is the species label, $+$ for positrons and $-$ for electrons, with $q_{\pm} = \pm e$. We linearize this equation with $f_s \rightarrow f_{0s} + \delta f_s$, $\mathbf{B} \rightarrow \delta \mathbf{B}$ and $\mathbf{E} \rightarrow \delta \mathbf{E}$, with the initial conditions downstream of the shock that tell us that $\delta \mathbf{E}$ and $\delta \mathbf{B}$ are small in the sense that $(\delta E^2 + \delta B^2)/8\pi nT \ll 1$. Then $\delta f_s/f_{0s}$ is also small. The linearized Vlasov equation is

$$\frac{\partial \delta f_s}{\partial t} + \mathbf{v} \cdot \nabla \delta f_s + \frac{q_s}{m_e} \left(\delta \mathbf{E} + \frac{\mathbf{v}}{c} \times \delta \mathbf{B} \right) \cdot \nabla_p f_{0s} = 0. \quad (2)$$

The plasma couples to the field through the Maxwell equations

$$\nabla \times \delta \mathbf{E} = -\frac{1}{c} \frac{\partial \delta \mathbf{B}}{\partial t}, \quad (3)$$

$$\nabla \times \delta \mathbf{B} = \frac{4\pi}{c} \delta \mathbf{j} + \frac{1}{c} \frac{\partial \delta \mathbf{E}}{\partial t}, \quad (4)$$

⁷ Note that we have defined the magnetic energy fraction $\epsilon_B \equiv B^2/4\pi\gamma_1 n_1 m c^2$ in terms of the *upstream* kinetic energy density, instead of the downstream thermal energy density as is a common practice in the GRB community (c.f., Piran 1999).

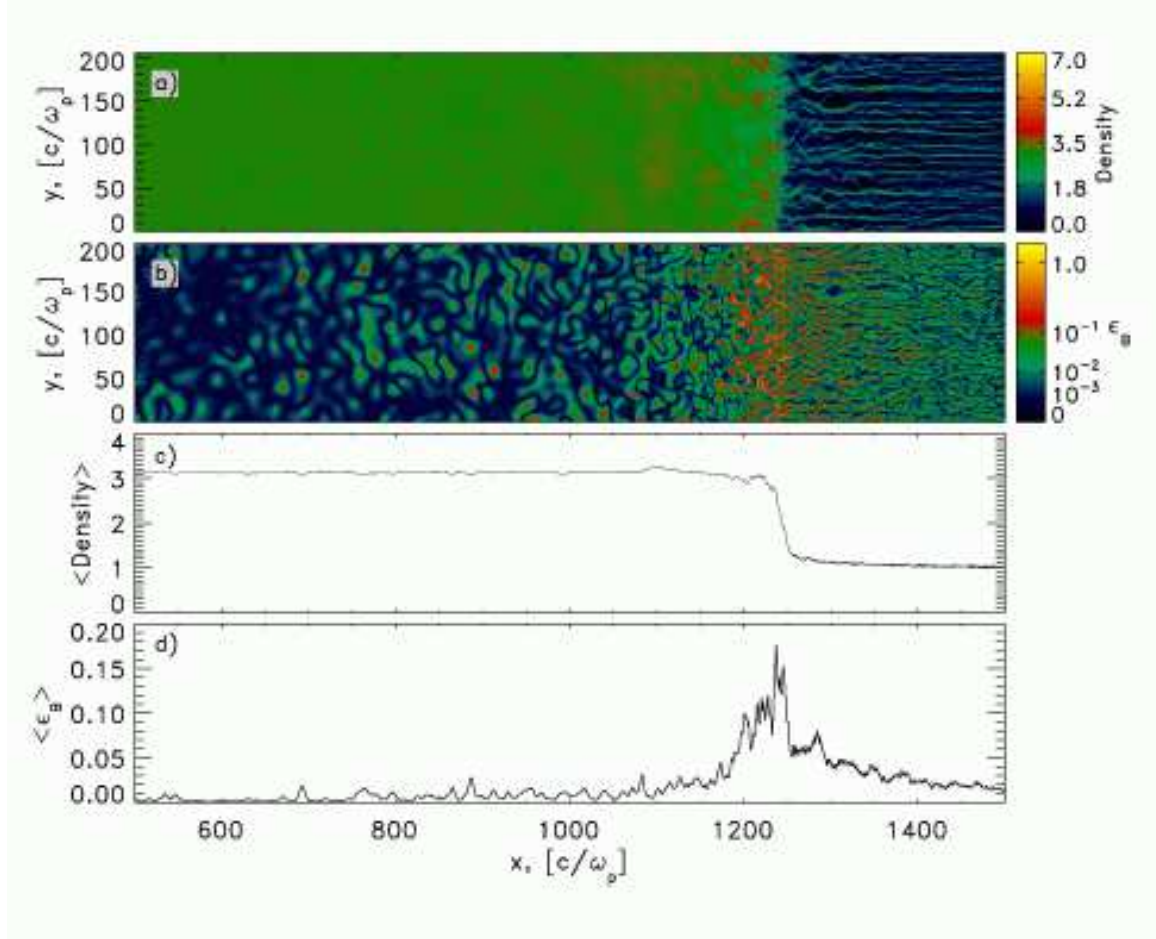


FIG. 1.— Snapshot of a region from a large 2D relativistic shock simulation. Incoming $\gamma = 15$ flow is moving to the left, while the shock moves to the right at $\approx 0.5c$. The postshock plasma is stationary in the frame of the simulation. a) Density structure in the simulation plane showing the plasma density enhancements in the foreshock region that steadily grow up to the shock transition region, where the density becomes homogeneous. Density is normalized in units of the plasma density far upstream. The density jump, $\langle n_2 \rangle / \langle n_1 \rangle = 3.13$, shown is exactly what is predicted by the hydrodynamic jump conditions for $\gamma_1 = 15$ in a 2D gas. b) Magnetic energy, normalized in terms of upstream energy of the incoming flow: $\epsilon_B = B^2 / 4\pi\gamma_1 n_1 mc^2$. The upstream magnetic filaments, which can be visualized as sheets coming out of the page, that are formed by the Weibel instability reach a peak just before the shock. These filaments become clumps of magnetic field, which can be visualized as cross-sections of loops that are transverse to the page in the downstream region, where they slowly decay away. Note that the B-field, which is organized into upstream filaments or downstream clumps, always points in or out of the page. A power law scaling, $\epsilon_B^{1/4}$, was applied to stretch the color table to show weak field regions; this is reflected in the colorbar. c) Plasma density averaged in the transverse direction as a function of the distance along the flow. d) Magnetic energy density averaged in the transverse direction, as a function of distance along the flow.

where $\delta \mathbf{j} = \sum_s q_s \int \mathbf{v} \delta f_s d^3p$ is the current density.

We orient coordinates so that $\delta \mathbf{E}$ is along x , the wave vector lies along y , and $\delta \mathbf{B}$ is along z . Assuming a wave solution with amplitudes $\propto \exp(-i\omega t +iky)$, equation (2) becomes

$$i(kv_y - \omega)\delta f_s + \frac{q_s}{m_e} \left(\delta E + \frac{v_y}{c} \delta B \right) \frac{\partial f_{0s}}{\partial p_x} - \frac{q_s}{m_e} \frac{v_x}{c} \delta B \frac{\partial f_{0s}}{\partial p_y} = 0. \quad (5)$$

Using equation (3) to eliminate δE yields

$$\delta f_s = i \frac{q_s \delta B}{m_e k c} \left(\frac{\partial f_{0s}}{\partial p_x} + \frac{kv_x}{\omega - kv_y} \frac{\partial f_{0s}}{\partial p_y} \right). \quad (6)$$

Using (4) yields

$$i(\omega^2 - k^2 c^2) \delta B = -4\pi k c \delta j. \quad (7)$$

Using (6) in the definition of δj yields

$$\delta j = -i\chi \omega \delta E \quad (8)$$

where χ is the plasma susceptibility,

$$4\pi\chi = \sum_s \frac{\omega_{p,\text{NR},s}^2}{\omega^2} \int v_x \left(\frac{\partial}{\partial p_x} + \frac{kv_x}{\omega - kv_y} \frac{\partial}{\partial p_y} \right) \frac{f_{0s}}{n_s} d^3p. \quad (9)$$

Here n_s is the number density of the electrons ($s = -$) or positrons ($s = +$) in the downstream plasma, $\omega_{p,\text{NR},s} = \sqrt{4\pi q_s^2 n_s / m_e}$ is the non-relativistic plasma frequency. We will assume by charge neutrality that in the downstream plasma $f_{0+} = f_{0-}$ and $n_+ = n_-$ so that the sum over equal mass species is trivial.

The dispersion relation for normal modes in the plasma plus electromagnetic field is

$$\frac{k^2 c^2}{\omega^2} - (1 + 4\pi\chi) = 0. \quad (10)$$

However, we emphasize that the linear relation between the currents and the electric field (eq.[8]) through the

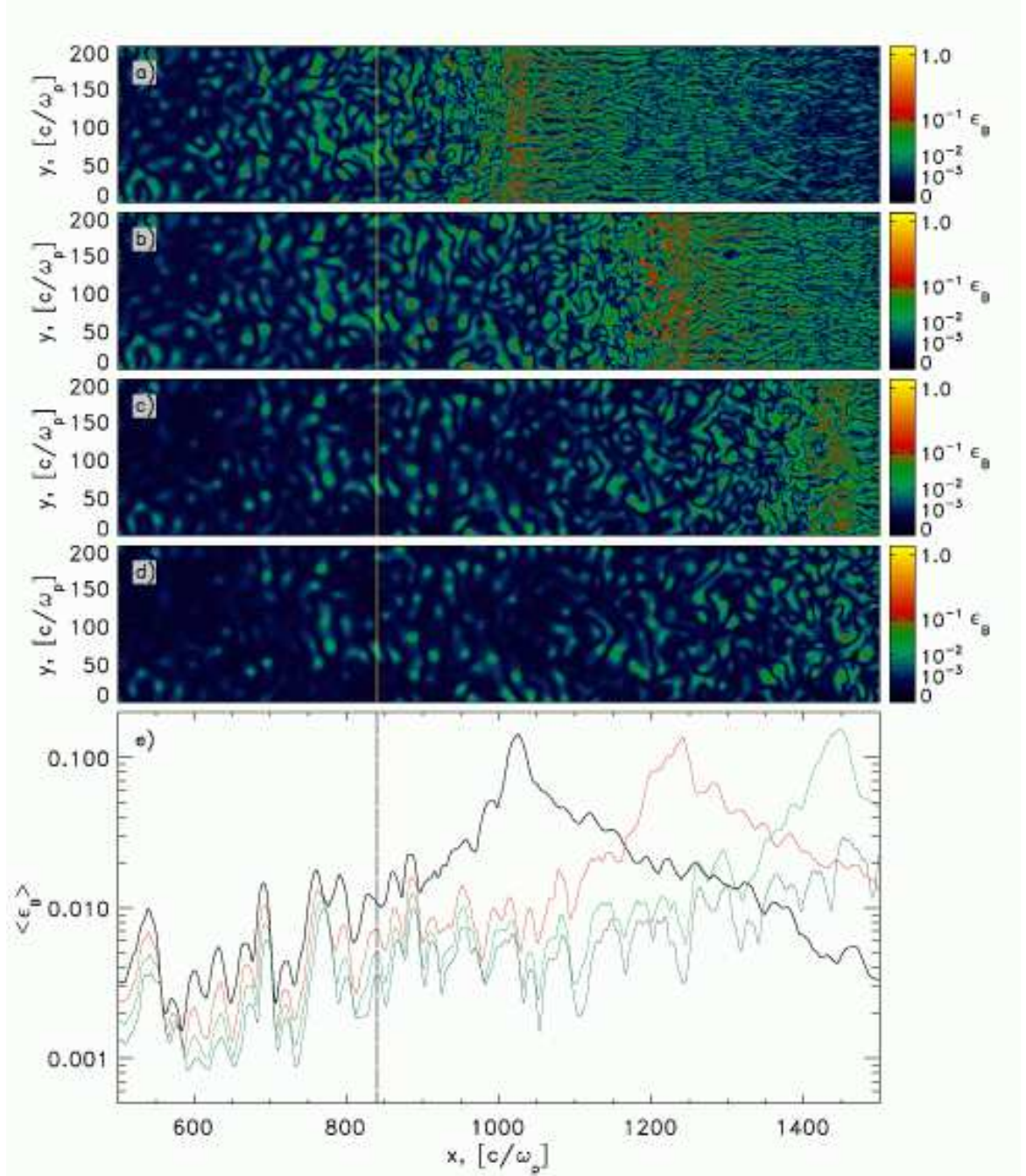


FIG. 2.— Cross-sectional views of the magnetic energy density for the same region as Figure 1, but at different times separated by $450 \omega_p^{-1}$ (a-d). The time of Figure 1 corresponds to panel b) in this plot. In panel e) we plot the B-field energy, averaged over y-axis as a function of distance along the flow direction with one curve for each of the top panels: (a) black, (b) red, (c) green, (d) blue. We also plot a vertical line at $x = 840c/\omega_p$ to define the region over which we perform a modal analysis in §3 and Figure 3.

susceptibility (9) applies to all (small amplitude) fluctuations, not only to normal modes.

We evaluate equation (9) for distribution functions that are isotropic in two and three dimensions in Appendix A. For a two-dimensional isotropic distribution function, we write $f_{0s}(\mathbf{p}) = f(p_{2d})g(p_z)$, where $p_{2d} = \sqrt{p_x^2 + p_y^2}$ and perform the integral over p_z such that $\int g(p_z)dp_z = 1$. For a three-dimensional isotropic distribution function, we write $f_{0s}(\mathbf{p}) = f_{0s}(p_{3d})$, where

$p_{3d} = \sqrt{p_x^2 + p_y^2 + p_z^2}$. In the three-dimensional case, we confirm Mikhailovskii's (1979) result for a relativistic isotropic plasma. As we show explicitly in equation (A5), subluminal waves ($\omega_r < kc$) are damped, where $\omega_r = \Re(\omega)$. The basic physics is that of Landau damping (Stix 1992) or more precisely, phase mixing. For a subluminal wave in an isotropic relativistic plasma with $\omega_r/k < c$, there always exists some angle ϕ between the wave vector k and a particle's momentum where a particle moving with speed $c\beta$ is in phase with the field

component, i.e., $\beta \cos \phi = \omega_r/kc$.

When the phase velocity of the field fluctuations is very small compared to the thermal speeds of the particles (which includes the zero wave velocity case, $\Re(\omega) = 0$), Landau damping takes on the character of simple phase-mixing. The currents, which support the field fluctuations, are composed of particles. These current carrying particles have random motions which carry them out of the magnetic structure, which the currents initially support. As a result, these currents and their magnetic field fluctuations are disorganized (or damped) on the transit times of the particles across the field fluctuations. It should be emphasized that the formal theory includes both this phase mixing limit of the damping process and the limit in which the phase 4-speeds $\beta_p/\sqrt{1-\beta_p^2}$, ($\beta_p \equiv \Re\omega/kc$), of the fields' Fourier components are high compared to the particles' random 4-speeds $\beta/\sqrt{1-\beta^2}$. The applicable limit depends on whether the wave phase 4-velocity is large or small compared to the mean 4-velocity of the particles in the distribution function. Hammett, Dorland & Perkins (1992) present a simple picture of this process in the case of non-relativistic electrostatic waves. Arons, Norman & Max (1977) show how phase mixing works for electromagnetic waves in a relativistic Maxwellian plasma. In any case, the end result is that there is a net power flow from fields to particles, i.e. the fields decay, which we will demonstrate explicitly below.

We now study the action of such a plasma on an arbitrary field of initial B-field perturbations as generated by the Weibel mediated shock. We evaluate equation (9) numerically for two and three dimensions setting $\omega_r = 0$, because of the non-propagating nature of the magnetic clumps, which we infer from visual inspection of the simulations. In the limit $k \ll \omega_p/c$, we find:

$$4\pi\chi \approx \begin{cases} i \frac{\omega_p^2}{|k|c\omega} & 2D \\ i \frac{\pi}{4} \frac{\omega_p^2}{|k|c\omega} & 3D \end{cases}. \quad (11)$$

Note that the 2D and 3D results only vary by a numerical factor. Hence, long wavelength modes have the same qualitative behavior in two and three dimensions.

The plasma susceptibility, which we calculate in Appendix A (see also eq.[11]), can be utilized to calculate the evolution, i.e., the damping or growth, of an initial field of fluctuations. Appendix B contains this calculation in more detail; the result is

$$\frac{d|\delta B_k|^2}{dt} = -2\gamma_k |\delta B_k|^2, \quad (12)$$

where $\gamma_k = (kc)^2 \omega^{-1} \Im(4\pi\chi)^{-1}$ (see also eq.[B8]). The asymptotic forms of χ from equation (11) for 3D and 2D gives (see also eq.[B9])

$$\gamma_k = \begin{cases} \frac{|kc|^3}{\omega_p^2} & 2D \\ \frac{4}{\pi} \frac{|kc|^3}{\omega_p^2} & 3D \end{cases}. \quad (13)$$

We now compare the expectations from linear response theory to the numerical simulations. We begin by taking the Fourier transform of δB from our 2D numerical simulations from a downstream region where the shock

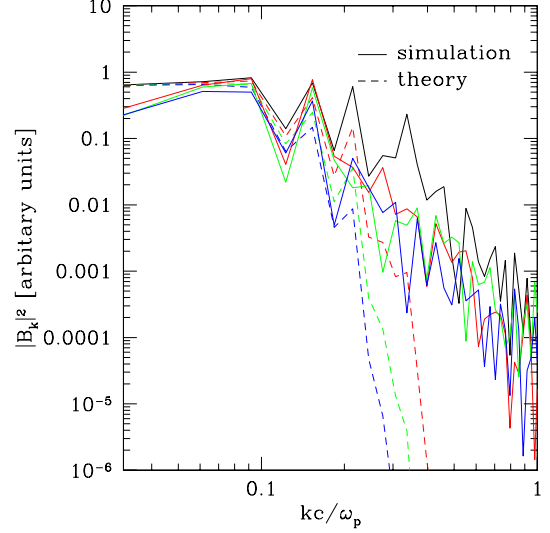


FIG. 3.— Spectral evolution of magnetic field from the slice at $840c/\omega_p$ from Fig. 2. Initial field spectrum (black solid line) is plotted after $450 \omega_p^{-1}$ (red), $900 \omega_p^{-1}$ (green), and $1350 \omega_p^{-1}$ (blue) based on simulation data. Dashed curves represent analytic evolution of the initial field and overpredict decay of short-wavelength structures.

is fully developed, i.e., behind the shock front at $x = x_0$,

$$\delta B(x_0, y) = \frac{1}{\sqrt{2\pi}} \int dk_y \delta B_{k_y}(x_0) \exp(ik_y y) \quad (14)$$

We evolve δB_{k_y} in accordance to equation (12) using the asymptotic forms in equation (13) and compare our analytically evolved spectra with the numerical simulation at later times. In Figure 3, we take the initial data from a region at $x_0 = 840c/\omega_p$, which we marked with a line in Figure 2. To accumulate sufficient statistics, we average the fields over $14c/\omega_p$ in the flow direction. We evolve these spectra for 450 (red), 900 (green), and $1350 \omega_p^{-1}$ (blue) using equation (13) and compare this to snapshots taken from our numerical simulations at these times. Theory and simulation agree at very low wavenumber ($k_y c/\omega_p \lesssim 0.2$). However, theory overpredicts the cutoff in power at larger k . The discrepancy suggests that linear theory is insufficient to describe the nature of downstream magnetic turbulence and that additional physics is needed (see §4).

The lack of power in short wavelength modes suggests that the total B-field is determined by long wavelength modes. We now use equation (12) to find a simple decay law for the total B-field:

$$\delta B(x_0, y, t) = \frac{1}{\sqrt{2\pi}} \int dk_y \delta B_{k_y}(x_0) \exp(ik_y y - \gamma_k t), \quad (15)$$

where $\delta B_{k_y}(x)$ is defined in equation (14). Inserting equation (13) into (15) and integrating, with $\delta B_{k_y} = a k_y^p$, where p is the long wavelength spectral index and a normalizes the amplitude, we find

$$\delta B(x_0, y, t) = \frac{1}{\sqrt{2\pi}} a \int_{k_0}^{\infty} dk_y k_y^p \exp\left(-\alpha \omega_p t \left(\frac{k_y c}{\omega_p}\right)^3\right) \quad (16)$$

$$\approx \frac{1}{3\sqrt{2\pi}} a \left(\frac{\omega_p}{c}\right)^{p+1} \Gamma\left(\frac{p+1}{3}\right) \left(\frac{1}{\alpha \omega_p t}\right)^{(p+1)/3} \quad (17)$$

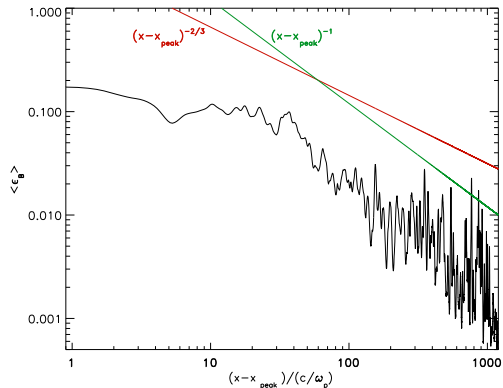


FIG. 4.— Magnetic energy density (in units of upstream kinetic energy) as a function of position downstream of the shock. A broken power law proportional $(x - x_{\text{peak}})^{-2/3}$ fits well at early times, but a $(x - x_{\text{peak}})^{-1}$ power law fits better at later times.

where we have taken $y = 0$ without loss of generality, $\alpha = 4/\pi$ in 3D and $\alpha = 1$ (2D), k_0 is small such that $\omega_p t (k_0 c / \omega_p)^3 \approx 0$, and Γ is the gamma function. Note that ω_p is for the downstream plasma frequency. However, this detail is irrelevant in terms of determining the power law as a function of t . Setting k_0 to be small is a safe approximation in the simulations, and of course is excellent in much larger astrophysical systems. Thus if the initial spatial spectrum is a power law in wave number $|\delta B_k|^2 \propto k^{2p}$, then the theory predicts $\delta B^2 \propto t^{-2(p+1)/3}$.

We study the region immediately following the peak of magnetic energy in the shock front (where it reaches $\delta B^2 = B_{\text{max}}^2$) at x_{peak} and plot its value as a function of position in the postshock region. For a shock moving at constant velocity, we have $x_{\text{peak}} - x \propto t$. Hence $\delta B^2 \propto (x_{\text{peak}} - x)^{-2(p+1)/3}$. Our numerical simulations are extremely suggestive that the magnetic energy density follows the $p = 0$, $\epsilon_B = \delta B^2 / 8\pi \propto t^{-2/3}$ decay expected for an initially flat magnetic spectrum at early times, then steepens to a t^{-1} decay at later times as shown in Figure 4, until the noise finally swamps the signal.⁸ This t^{-1} decay rate would imply an initial spatial index of $p = 1/2$ at low wavenumber, though our analysis of additional simulations with a large transverse spatial scale suggest $p = 0$. The difference in the index of the decay law expected from the theory and measured from the simulations may be due to magnetic trapping (see §4). Gruzinov (2001b) offered an alternative explanation of t^{-1} decay of the magnetic energy density observed in 2D simulations of Weibel instability in counterpropagating pair plasmas. In that simulation the beams were moving perpendicular to the simulation plane⁹. In order to explain the field decay, Gruzinov (2001b) had to

⁸ Gruzinov (2001a) performed shock simulations (initiated by a collision between two e^\pm plasmas), which show decay of the magnetic energy averaged over the dimension across the flow similar to the early phases of the decay we report here.

⁹ Being orthogonal to the direction of motion these simulations did not form a shock and retained some counterstreaming at late times. In contrast, our simulations lose the counterstreaming once the shock forms.

assume that the magnetic structures increase their size at the Alfvén velocity. In our shock simulations, the downstream magnetic structures do not significantly expand (§2), hence the similarity of decay law between the two simulations is likely a coincidence. The picture of filament expansion and merging of Gruzinov (2001b) is likely valid very close to the shock, but is not observed in the longer evolution of the downstream plasma.

4. MAGNETIC TRAPPING

Our simulations and theory suggest power law t^{-q} with $q \sim 1$ temporal decay of the total magnetic energy density in rough agreement with each other. However, linear theory and numerical simulations disagree on the decay rate for short wavelengths, which hinders a determination of the ultimate fate of the fields on times longer than several thousand plasma periods. This discrepancy may arise from the nonlinear effects of magnetic trapping. Particles in the magnetic fields do not follow straight line trajectories that are weakly perturbed, but are partially trapped and strongly deflected. We illustrate this point from following test particles' orbits in numerical simulations in Figure 5. The test particles suffer large deflections from straight-line orbits as they encounter magnetic clumps. Therefore, the Larmor radii of many of the test particles are of the same order of the sizes of these clumps or smaller. Indeed closer inspection of some of the test particle orbits that are embedded inside the clumps suggests that they are completely trapped.

These strong departures from weakly perturbed particle dynamics may be the cause of the decreased damping at large wavenumber found in the simulations, compared to the predictions of unmagnetized plasma theory. Magnetic trapping may also modify the decay of magnetic fields at small wavenumber, leading perhaps to a different decay law instead of expected $t^{2/3}$ decay law that we find from our simple linear theory (eq.[17] with $p = 0$). The temporary (and permanent, for some particles) binding of particles to the spatially intermittent magnetic fields reduces the effect of rapid phase mixing central to the unmagnetized plasma damping theory. Magnetic trapping already plays a critical role in the saturation of the initial Weibel instability at the shock transition region (Kato 2005; Davidson *et al.* 1972). Our analysis suggests that trapping also plays an important role downstream even though the *average* magnetic amplitudes are greatly reduced from the shock transition region - the essential point is that within the isolated filaments, the magnetic pressure is not small. The problem of the damping of isolated magnetic structures in a plasma with partial magnetization illustrated in Figure 5 will be the subject of a separate investigation.

5. DISCUSSION

We have studied the downstream evolution of magnetic turbulence in the context of a collisionless e^+e^- shock both analytically and numerically. Our large scale 2D simulations show the formation of filaments in the foreshock region which merge and grow until they reach the shock transition region. Past the shock transition region, these filaments break up into magnetic clumps in a quasi-homogenous medium where the background particle distribution function is an isotropic Maxwellian.

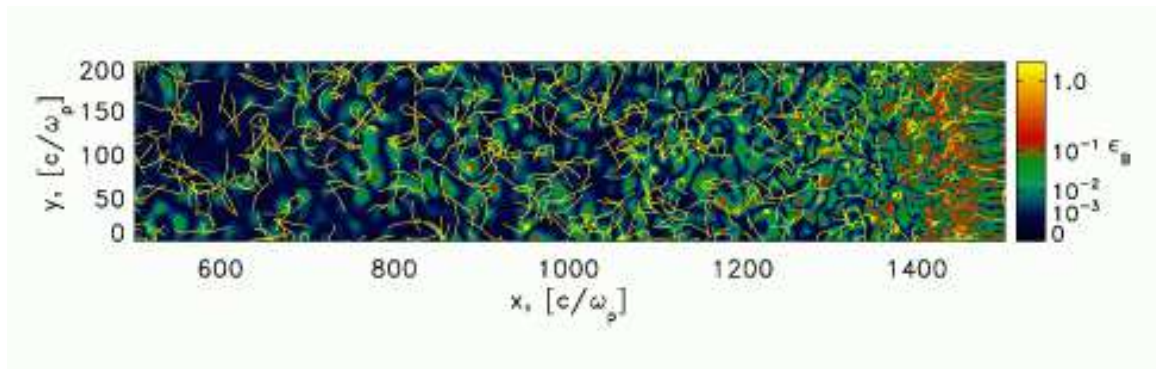


FIG. 5.— Segments of particle orbits from the high resolution 2D simulation overplotted on a snapshot of magnetic energy downstream of the shock. Typical sizes of magnetic clumps are $10\text{--}20\ c/\omega_p$. The shock is near the right boundary of this slice, moving to the right. The large angle deflections in particle orbits suggest the Larmor radii of many particles in this slice are of the same order as the sizes of the magnetic clumps.

In such a background, we showed that magnetic energy will decay like t^{-q} with $q \sim 1$ due to untrapped particle phase mixing, which is broadly consistent with our numerical simulations. In detail, the theoretical decay rates depend more strongly on wavelength than is seen in the numerical experiments. We suggested that magnetic trapping may play an important role in resolving this discrepancy. Trapping can lead to MHD-like behavior and possible long time persistence of some of the magnetic energy in spatially intermittent, more strongly magnetized subregions. This effect is a subject of further study.

Magnetic field decay may be alleviated via an inverse cascade from small scales to large scales. An inverse cascade via current filament merging operates strongly in the *foreshock* region (Silva *et al.* 2003; Spitkovsky 2005). However, it is unclear if this picture can be applied to the downstream region. The magnetic filaments so prevalent in the upstream region are gone and are replaced by isolated magnetic clumps (loops), a result common to both 2D and 3D simulations. Filament merging does occur, but is confined to the foreshock, where the filaments exist. We see little evidence of merging magnetic clumps. This is reinforced by Katz *et al.* (2007), who suggest via self-similar arguments that the inverse cascade does not operate downstream of the shock. Hence, the magnetic energy should damp away in the downstream region.

We have not studied in detail how these magnetic clumps are confined in the downstream plasma. However, Fujita *et al.* (2006) have found these same magnetic clumps in simulation of the non-relativistic Weibel instability that is appropriate for galaxy clusters. In this case, they argue that pressure of the external medium confines these magnetic clumps. The strong perturbation from straight line motion, which we studied in §4 for test particles, suggest that the magnetic clumps in our simulation are also sensitive to momentum transfer between particles and itself. That is, the magnetic clumps in our simulations are also confined by external pressure.

Whatever the final fate of the spatially intermittent fields, our study of the nature of e^+e^- shocks suggests that the belief in the persistence of Weibel generated magnetic fields with strengths comparable to those appearing within the shock transition is overly optimistic. Magnetic field energies tend to decline rapidly after

about a few hundred plasma skin depths. Only the very long term evolution is still open to some question, i.e., does $\langle \epsilon_B \rangle$ settle at some value smaller than 10^{-3} , or does the spatially intermittent magnetic field decline to zero?

The rapid decay suggested by our analysis puts severe constraints on the synchrotron emission mechanisms for GRBs. The width of the emitting region is $\sim 10^9 c/\omega_p$ (Piran 2005b), which is much larger than the region over which we expect magnetic fields to persist. However, decaying magnetic fields may not be inconsistent with GRB observations. Pe’er & Zhang (2006) suggest that the prompt emission from the internal shock may be more consistent with a decaying magnetic field component rather than a persistent field component. A field that persists over a scale of $10^4 - 10^5$ plasma skin depths fits the spectra better at low-energies than a field that persists over the entire thickness of the shell (10^9 plasma skin depths). Small magnetized regions may also be important in the context of the afterglow (Rossi & Rees 2003).

In young pulsar wind nebulae, post shock magnetic fields averaged over the whole latitudinal extent of the observed emission tori have energy densities of a few percent of the post shock plasma energy density. It is possible that weaker magnetic fields exist near the midplane of the equatorial flow, a region of particular interest to the conversion of flow energy into the observed nonthermally emitting spectra of e^\pm . If so, the Weibel mediated shock dynamics studied here may be of relevance to these systems’ behavior.

It is also possible that weak systematic upstream magnetic fields are of essential importance, and that shocks in completely unmagnetized plasmas are an oversimplification. Suprathermal particle generated at the relativistic shock front may alter the basic physics of the collisionless shock, if a mean field is present. Milosavljevic and Nakar (2006b) argue accelerated particles streaming into the *upstream* magnetized medium can drive long wavelength, magnetized turbulence with $\delta B/B \gg 1$, which might persist into the downstream and provide the magnetization required in phenomenological models of GRB and PWN emission. Then the shock mediated by Weibel turbulence becomes a subshock within a much larger extended structure, responsible only for thermalizing the bulk of the flow and injecting the particles that are Fermi

accelerated in the turbulence generated by high energy particle streaming. This is a relativistic version of Bell's (1978) (also see Bell 2004, 2005) picture of particle acceleration in non-relativistic shocks.

Finally, we briefly mention the extension of this theory to electron-ion plasmas. Let us presume initially that the ions and electrons are isotropic but remain decoupled, i.e., a two-temperature relativistic plasma. Equation (11) becomes

$$\chi \approx i \frac{\pi}{4} \frac{\omega_{p,i}^2 + \omega_{p,e}^2}{|k|c\omega}, \quad (18)$$

where $\omega_{p,i}^2 = 4\pi n_i e^2 / \gamma_i m_i$ is the plasma frequency of the ions, γ_i is the Lorentz factor associated with the ion temperature, $\omega_{p,e}^2 = 4\pi n_e e^2 / \gamma_e m_e$ is the plasma frequency of the electrons, and γ_e is the Lorentz factor associated with the electron temperature. Depending on the relative values of the electron temperature and ion temperature, one term may dominate. However, initial large-scale simulations of ion-electron collisionless shocks suggest that both reach roughly equipartition with each other (Spitkovsky 2007), thereby reproducing the physics of the e^\pm shock. In this case, the relativistic electrons

and ions contribute equally to the decay rate because thermal equipartition prevails, i.e., $m_e \gamma_e = m_i \gamma_i$. Thus, the electron-ion plasma has the same dynamics as the electron-positron plasma.

We thank S. Cowley, D. Kocelski, M. Milosavljevic, A. Pe'er and E. Quataert for useful discussions. P.C. and J.A. thank the Institute for Advanced Study for its hospitality; P.C. also thanks the Canadian Institute for Theoretical Astrophysics for similar hospitality. P.C. is supported by the Miller Institute for Basic Research. J.A. has benefited from the support of NSF grant AST-0507813, NASA grant NNG06G108G, and DOE grant DE-FC02-06ER41453, all at UC Berkeley; by the Department of Energy contract to the Stanford Linear Accelerator Center no. DE-AC3-76SF00515; and by the taxpayers of California. A.S. is pleased to acknowledge that the simulations reported on in this paper were substantially performed at the TIGRESS high performance computer center at Princeton University which is jointly supported by the Princeton Institute for Computational Science and Engineering and the Princeton University Office of Information Technology.

APPENDIX

SUSCEPTIBILITY IN TWO AND THREE DIMENSIONS

In this section, we solve the susceptibility (eq.[9]) for two and three dimensional plasma. The 3D case (§A.1) has been previously solved by Mikhailovskii (1979) and we reproduce his result here for completeness. In addition, we present the 2D case (§A.2), which allows for a comparison to the two-dimensional simulations reported in this paper.

Three Dimensions

After summing over the electrons and positrons, equation (9) is

$$4\pi\chi = \frac{\omega_{p,\text{NR}}^2}{\omega^2} \int v_x \left(\frac{d}{dp_x} + \frac{kv_x}{\omega - kv_y} \frac{d}{dp_y} \right) \frac{f_0}{n} d^3p, \quad (A1)$$

where n is the number density of electrons and positrons. Since f_0 is isotropic and therefore independent of angle, we orient the spherical integral in a *non-standard manner* so that the pole points along the \mathbf{k} -vector, i.e., the y -axis. We find $\hat{\mathbf{p}} \cdot \hat{\mathbf{y}} = \cos \theta$ and $\hat{\mathbf{p}} \cdot \hat{\mathbf{x}} = \sin \theta \sin \phi$. So equation (A1) becomes

$$4\pi\chi = \frac{\omega_{p,\text{NR}}^2}{\omega^2 n} \int v \sin^2 \theta \sin^2 \phi \left(1 + \frac{\cos \theta}{\omega/kv - \cos \theta} \right) \frac{df_0}{dp} p^2 dp d\Omega, \quad (A2)$$

where $d\Omega = \sin \theta d\theta d\phi$. Performing the integral over ϕ and making the substitution $\zeta = \cos \theta$, we find

$$4\pi\chi = \frac{\pi \omega_{p,\text{NR}}^2}{\omega^2 n} \int v (1 - \zeta^2) \left(1 + \frac{\zeta}{\omega/kv - \zeta} \right) \frac{df_0}{dp} p^2 dp d\zeta. \quad (A3)$$

Integrating over ζ from -1 to 1, we find

$$4\pi\chi = \frac{2\pi \omega_{p,\text{NR}}^2}{\omega^2 n} \int p^2 dp \frac{df_0}{dp} v \left\{ \left(\frac{\omega}{kv} \right)^2 - \frac{\omega}{kv} \left[1 - \left(\frac{\omega}{kv} \right)^2 \right] \times \left[\frac{1}{2} \log \left(-\frac{1 + \omega/kv}{1 - \omega/kv} \right) \right] \right\}. \quad (A4)$$

Note that the logarithmic function will give an imaginary part when $\omega_r/kc\beta < 1$. This implies that waves whose phase velocity, ω_r/k , is small compared to the thermal speed of the background particles, $c\beta$, will be damped (also see §3). We pull this imaginary component out of the equation, which makes this damping more explicit, to find:

$$4\pi\chi = \frac{2\pi \omega_{p,\text{NR}}^2}{\omega^2 n} \int p^2 dp \frac{df_0}{dp} v \left\{ \left(\frac{\omega}{kv} \right)^2 - \frac{\omega}{kv} \left[1 - \left(\frac{\omega}{kv} \right)^2 \right] \times \left[\frac{1}{4} \log \left(\frac{1 + \omega/kv}{1 - \omega/kv} \right)^2 - i \frac{\pi}{2} \Theta(k^2 v^2 - \omega_r^2) \right] \right\}, \quad (A5)$$

where Θ is the unit step function (i.e., $\Theta(z) = 1$ for $\Re(z) \geq 0$ and $\Theta(z) = 0$ for $\Re(z) < 0$). Equation (A5) is precisely Mikhailovskii (1979)'s result. We now apply a three dimensional relativistic Maxwellian $f_0 \propto \exp(-E/kT)$, which is appropriately normalized, $\int d^3p f_0 = n$, and solve equation (A5) numerically. For the ultrarelativistic case $v \approx c$, we find a simple form in the limit $\omega_r \ll kc$:

$$4\pi\chi \approx i \frac{\pi}{4} \frac{\omega_p^2}{|k|c\omega}. \quad (\text{A6})$$

Two Dimensions

Starting from equation (A1), we assume $f_0 = f(p_{2d})g(p_z)$, where $p_{2d} = \sqrt{p_x^2 + p_y^2}$ and perform the integral over p_z . The resulting two dimensional analogue of equation (A1) is

$$4\pi\chi = \frac{\omega_{p,\text{NR}}^2}{\omega^2} \int v_x \left(\frac{d}{dp_x} + \frac{kv_x}{\omega - kv_y} \frac{d}{dp_y} \right) \frac{f}{n} d^2p, \quad (\text{A7})$$

where we have dropped the subscript “2d” from p . Defining $p_x = p \cos \theta$, $p_y = p \sin \theta$, and similarly for v_x and v_y , we find:

$$4\pi\chi = \frac{\omega_{p,\text{NR}}^2}{\omega^2 n} \int p dp \int_0^{2\pi} d\theta v \cos^2 \theta \left(1 + \frac{\sin \theta}{(\omega/kv) - \sin \theta} \right) \frac{df}{dp}. \quad (\text{A8})$$

We may transform the θ integral from 0 to 2π to a contour integral over the unit circle by making the appropriate substitutions (Carrier, Krook, & Pearson 1983)

$$\cos \theta \rightarrow \frac{1}{2} (z + z^{-1}), \sin \theta \rightarrow \frac{1}{2i} (z - z^{-1}) \quad (\text{A9})$$

$$d\theta \rightarrow \frac{dz}{iz}, \int_0^{2\pi} \rightarrow \int_{\Gamma}, \quad (\text{A10})$$

where Γ is the unit circle. After a bit of algebra, we find

$$4\pi\chi = \frac{\omega_{p,\text{NR}}^2}{\omega^2 n} \int v \frac{df}{dp} p dp \int_{\Gamma} \frac{-i}{4} dz (z^2 + 2 + z^{-2}) \frac{(2i\omega/kv)}{(2i\omega/kv)z - z^2 + 1}. \quad (\text{A11})$$

The singular points in this equation are $z_{\pm} = (i\omega/kv) \mp \sqrt{1 - (\omega/kv)^2}$. We perform the contour integral by noting that only the z_- root contributes for $(\omega/kv)^2 < 1$:

$$4\pi\chi = -i \frac{2\pi\omega_{p,\text{NR}}^2}{\omega kn} \int \sqrt{1 - \left(\frac{\omega}{kv}\right)^2} \frac{df}{dp} p dp. \quad (\text{A12})$$

We apply a two dimensional relativistic Maxwellian $f \propto \exp(-E/kT)$, where f is appropriately normalized, i.e. $\int f d^2p = n$. Expanding to lowest order in ω/kv , we find:

$$4\pi\chi \approx i \frac{\omega_p^2}{|k|c\omega}. \quad (\text{A13})$$

DECAY OF AN INITIAL FIELD OF FLUCTUATIONS

The plasma susceptibilities (eq.[11]) define the linear response of the plasma. These susceptibilities are complex and hence the electric permittivity $\epsilon = 1 + 4\pi\chi$ is also complex. The implications of Poynting's theorem for the propagation of small amplitude waves and fluctuations in such a medium have been described in many texts and monographs (e.g., Bekefi 1966, Melrose and McPhedran 1991, Stix 1992). For completeness, we give a brief discussion of the theory behind expression (12).

We begin with Poynting's theorem:

$$\frac{\partial}{\partial t} \left(\frac{\delta B^2 + \delta E^2}{8\pi} \right) + \nabla \cdot \mathbf{S} = -\delta \mathbf{j} \cdot \delta \mathbf{E}, \quad (\text{B1})$$

where $\mathbf{S} = (c/4\pi) \mathbf{E} \times \mathbf{B}$ is the Poynting vector. We assume field energy is distributed uniformly in our uniform plasma, so $\nabla \cdot \mathbf{S} = 0$, i.e., there is no transport of energy spatially. In addition, for nonpropagating Weibel modes, $\delta E \ll \delta B$. Thus, we find a simplified expression:

$$\frac{\partial}{\partial t} \left(\frac{\delta B^2}{8\pi} \right) = -\delta \mathbf{j} \cdot \delta \mathbf{E}. \quad (\text{B2})$$

Writing the fields with truncated amplitudes

$$\delta B_{TV}(\mathbf{r}, t) = \begin{cases} \delta B, & t \in (-T/2, T/2), |\mathbf{r}| \in V, \\ 0, & t \notin (-T/2, T/2), |\mathbf{r}| \notin V, \end{cases} \quad (\text{B3})$$

with $\delta B_{TV} = 0$ when the coordinates are outside of the volume, V , and time is outside of the interval $(-T/2, T/2)$. Thus, we can define space-time averages of the fields while still expressing them in terms of convergent Fourier transforms. We write the Fourier transforms as

$$\delta j_{k\omega} = \int d^3k \int_{-\infty}^{\infty} d\omega \delta j_{TV} \exp(i\mathbf{k} \cdot \mathbf{r} - i\omega t). \quad (\text{B4})$$

We express the field energy density and the $\delta j \cdot \delta E$ work in terms of the Fourier amplitudes and then average over time and space. Taking T and V to ∞ , we integrate over the resulting δ -functions to find

$$\frac{\partial}{\partial t} \left\langle \frac{\delta B^2}{8\pi} \right\rangle = \int d^3k \int d\omega \frac{1}{2} \langle \delta j_{k\omega} \delta E_{k\omega}^* + c.c. \rangle, \quad (\text{B5})$$

where $\langle \rangle$ represents the space time average over the fluctuation wavelengths and variability times and *c.c.* is the complex conjugate. We apply the same Fourier transform to δB and apply the same average over time and space. We use the linear response (eq.[8]) $\delta E_{k\omega} = (i/\chi\omega)\delta j_{k\omega}$ to find

$$\frac{1}{8\pi} \frac{\partial \langle |\delta B_{k\omega}|^2 \rangle}{\partial t} = -\Im(\omega\chi)^{-1} \langle |\delta j_{k\omega}|^2 \rangle. \quad (\text{B6})$$

Now using $\delta j_{k\omega} = ikc\delta B_{k\omega}/4\pi$, we find

$$\frac{\partial \langle |\delta B_{k\omega}|^2 \rangle}{\partial t} = -2\gamma_{k\omega} \langle |\delta B_{k\omega}|^2 \rangle, \quad (\text{B7})$$

where $\gamma_{k\omega}$ is the damping rate or

$$\gamma_{k\omega} = \frac{(kc)^2}{\omega} \Im(4\pi\chi)^{-1}. \quad (\text{B8})$$

Equation (B7) is a specific form of the fluctuation-dissipation theorem (Thompson and Hubbard 1960) from which the same result can be derived.

Equations (B7) and (B8) define the evolution of magnetic energy in terms of the linear response. For notational simplicity we reduce $k\omega \rightarrow k$ in the rest of the text. We obtain simple forms for γ_k , using the asymptotic forms of $4\pi\chi$ from equation (11) for 3D and 2D. We find for $kc \ll \omega_p$:

$$\gamma_k = \begin{cases} \frac{|kc|^3}{\omega_p^2} & 2\text{D} \\ \frac{4}{\pi} \frac{|kc|^3}{\omega_p^2} & 3\text{D} \end{cases}. \quad (\text{B9})$$

The cubic dependence on wavenumber in equation (B9) suggests short wavelength modes are very strongly damped, while longer wavelength modes can survive much longer.

Taking the general form of $4\pi\chi$ for 2D and 3D from equation (A5) and (A12), we numerically compute the damping rate from equation (B8) for Weibel modes where $\omega_r = 0$, because of the non-propagating nature of the downstream magnetic clumps. We show the results in Figure B6. Also plotted are the simple forms for γ_k from equation (B9). Though, the asymptotic forms are only valid for $kc/\omega_p \ll 1$, the numerical and asymptotic results are in excellent agreement throughout. Thus for simplicity, we use equation (B9) (also eq.[13] in the main body) for the damping rates.

REFERENCES

- Arons, J., Norman, C. A., & Max, C. E. 1977, *Phys. Fluids*, 20, 1302
- Bekefi, G. 1966, “Radiation Processes in Plasmas” (John Wiley: New York)
- Bell, A. R. 1978, *MNRAS*, 182, 147
- Bell, A. R. 2004, *MNRAS*, 353, 550
- Bell, A. R. 2005, *MNRAS*, 358, 181
- Birdsall, C. K. & Langdon, A. B. 1991, “Plasma Physics via Computer Simulations” (McGraw-Hill: New York)
- Buneman, O. 1993 in “Computer Space Plasma Physics”, Terra Scientific, Tokyo, 67
- Carrier, G. F., Krook, M., & Pearson, C. E. 1983, “Functions of a Complex Variable : Theory and Technique” (Hod Books: Ithaca)
- Coroniti, F. V. 1990, *ApJ*, 349, 538
- Davidson, R. C., Hammer, D. A., Haber, I., & Wagner, C. E. 1972, *Phys. Fluids*, 15, 317
- Frederiksen, J. T., Hededal, C. B., Haugbølle, T., & Nordlund, . 2004, *ApJ*, 608, L13
- Gallant, Y. A., Hoshino, M., Langdon, A. B., Arons, J., & Max, C. E. 1992, *ApJ*, 391, 73
- Gruzinov, A. 2001a, submitted to *ApJ*, astro-ph/0111321
- Gruzinov, A. 2001b, *ApJ*, 563, L15
- Gruzinov, A. & Waxman E. 1999, *ApJ*, 511, 852
- Hammett, G. W., Dorland, W., & Perkins, F. W. 1992, *Phys. Fluids* B, 4, 2052
- Hededal, C. B., Trier Frederiksen, J., Haugboelle, T., & Nordlund, A. 2005, Neutrinos and Explosive Events in the Universe, Proceedings of the 14th Course of the International School of Cosmic Rays Astrophysics, a NATO Advanced Study Institute, held in Erice, Italy, 2-13 July 2004. Edited by Maurice M. Shapiro, Stanev Todor, and John P. Wefel.
- Jackson, J. D. 1999, “Classical Electrodynamics” (John Wiley & Sons: New York)
- Kato, T. N. 2005, *Phys. Plasmas*, 12, 80705
- Katz, B., Keshet, U., & Waxman, E. 2007, *ApJ*, 655, 375
- Medvedev, M. V. & Loeb, A. 1999, *ApJ*, 526, 697
- Medvedev, M. V., Fiore, M., Fonseca, R. A., Silva, L. O.; Mori, W. B. 2005, *ApJ*, 618, L75
- Melrose, D.B., and McPhedran, R.C. 1991, “Electromagnetic Processes in Dispersive Media” (Cambridge: Cambridge University Press)
- Milosavljevic, M., Nakar, E., & Spitkovsky, A. 2006, *ApJ*, 637, 765
- Milosavljevic, M. & Nakar, E. 2006a, *ApJ*, 641, 978
- Milosavljevic, M. & Nakar, E. 2006b, *ApJ*, 651, 979

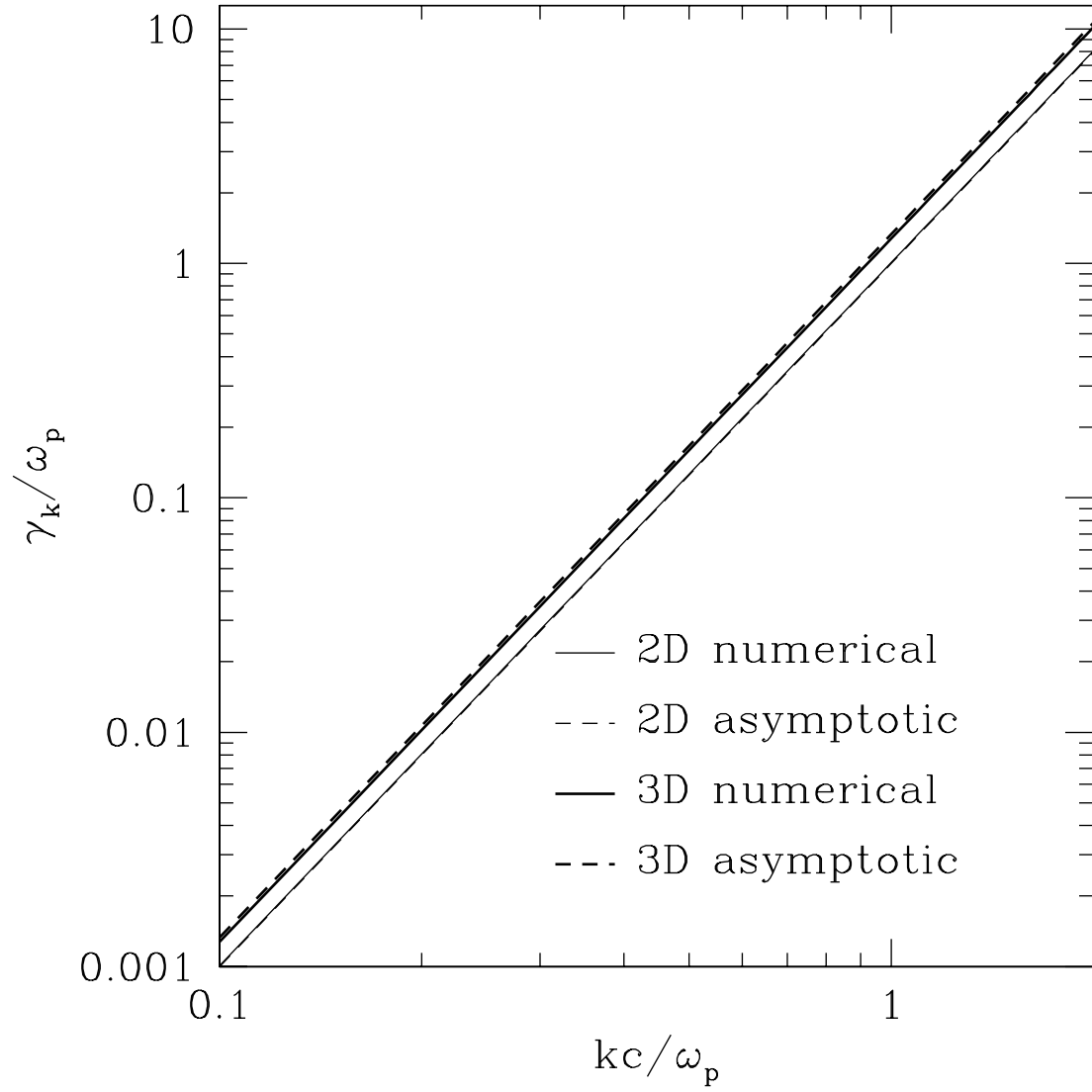


FIG. B6.— Damping rates of magnetic field as a function of kc/ω_p . We plot the damping rates numerically computed from equation (A5) and (A12) for 3D (thick solid line) and 2D (thin solid line) respectively. Also overplotted are the analytic forms of these expressions from equation (13) for 2D (thin dashed line) and 3D (thick dashed line).

- Mikhailovskii, A. B. 1979, *Plasma Phys.*, 22, 133
- Nishikawa, K.-I., Hardee, P., Richardson, G., Preece, R., Sol, H., & Fishman, G. J. 2003, *ApJ*, 595, 555
- Nishikawa, K.-I., Hardee, P., Richardson, G., Preece, R., Sol, H., & Fishman, G. J. 2005, *ApJ*, 622, 927
- Pe'er, A. & Zhang, B. 2006, *ApJ*, 653, 454
- Piran, T. 2005a, *Rev. of Modern Phys.*, 76, 1143
- Piran, T. 2005b, *Magnetic Fields in the Universe*, Angra dos Reis, Brazil, Nov. 29-Dec 3, 2004, Ed. E. de Gouveia del Pino, AIP Conference Proceedings, v784 (New York:AIP), p164
- Rossi, E. & Rees, M. J. 2003, *MNRAS*, 339, 881
- Silva, L. O., Fonseca, R. A., Tonge, J. W., Dawson, J. M., Mori, W. B., & Medvedev, M. V. 2003, *ApJ*, 596, 121
- Spitkovsky, A. 2005, *AIP Conf. Proc.*, 801, 345; astro-ph/0603211
- Spitkovsky, A. 2007, submitted to *ApJ*; arXiv:0706.3126
- Stix, T.H. 1992, "Waves in Plasmas" (American Institute of Physics: New York)
- Thompson, W. B. & Hubbard, J. 1960, *Rev. of Modern Phys.*, 32, 714
- Weibel, E. S. 1959, *Phys. Rev. Lett.*, 2, 83
- Yoon, P. H., & Davidson, R. C. 1987, *Phys. Rev. A*, 35, 2718

